# Lithospheric structure, evolution and diamond prospectivity of the Rehoboth Terrane and western Kaapvaal Craton, southern Africa: Constraints from broadband magnetotellurics

M.R. Muller [a,*], A.G. Jones [a], R.L. Evans [b], H.S. Grütter [c], C. Hatton [d], X. Garcia [a], M.P. Hamilton [a,2], M.P. Miensopust [a,n], P. Cole [e], T. Ngwisanyi [f], D. Hutchins [g], C.J. Fourie [h], H.A. Jelsma [i], S.F. Evans [i,3], T. Aravanis [j], W. Pettit [k], S.J. Webb [l], J. Wasborg [m] and The SAMTEX Team [1]

[a] Dublin Institute for Advanced Studies, 5 Merrion Square, Dublin 2, Ireland
[b] Department of Geology and Geophysics, Woods Hole Oceanographic Institution, Clark South 263, 266 Woods Hole Road, Woods Hole, Massachusetts, 02543-1542, USA
[c] BHP Billiton World Exploration Inc., Suite 800, Four Bentall Centre, 1055 Dunsmuir Street, Vancouver, B.C., V7X 1L2, Canada
[d] MSA Geoservices, 20B Rothesay Avenue, Craighall Park, Johannesburg, South Africa
[e] Council for Geoscience, 280 Pretoria Street, Silverton, Pretoria 0001, South Africa
[f] Geological Survey of Botswana, Private Bag 14, Lobatse, Botswana
[g] Geological Survey of Namibia, 1 Aviation Road, Windhoek, Namibia
[h] Council for Scientific and Industrial Research, Pretoria, South Africa
[i] De Beers Group Services, Private Bag X01, Southdale 2135, South Africa
[j] Rio Tinto Mining and Exploration Ltd., 1 Research Avenue, Bundoora, 3081, Victoria Australia
[k] BHP Billiton, 6 Hollard Street, Johannesburg 2001, South Africa
[l] University of the Witwatersrand, School of Geosciences, Jan Smuts Avenue, Johannesburg 2050, South Africa
[m] ABB Power Technologies ABB–HVDC, Ludvika, SE-77180, Sweden
[n] National University of Ireland, Galway, University Road, Galway, Ireland

## ARTICLE INFO

## ABSTRACT

A 1400 km-long, 2-D magnetotelluric (MT) profile, consisting of 69 sites at 20 km intervals, across the western part of the Archaean Kaapvaal Craton, the Proterozoic Rehoboth Terrane and the Late Proterozoic/Early Phanerozoic Ghanzi-Chobe/Damara Belt reveals significant lateral heterogeneity in the electrical resistivity structure of the southern African lithosphere. The lithospheric structures of the Rehoboth Terrane and Ghanzi-Chobe/Damara Belt have not been imaged previously by geophysical methods. Temperature is the primary control on the resistivity of mantle minerals, and the MT derived lithospheric thicknesses therefore provide a very reasonable proxy for the "thermal" thickness of the lithosphere (i.e., the thickness defined by the intersection of a conductive geotherm with the mantle adiabat), allowing approximate present-day geotherms to be calculated. The work indicates the following present-day average lithospheric thicknesses, to a precision of about $\pm$ 20 km, for each of the terranes traversed (inferred geotherms in brackets): Eastern Kimberley Block of the Kaapvaal Craton 220 km (41 mW m$^{-2}$), Western Kimberley Block 190 km (44 mW m$^{-2}$), Rehoboth Terrane 180 km (45 mW m$^{-2}$) and Ghanzi-Chobe/Damara Belt 160 km (48 mW m$^{-2}$). A clear relationship between the electrical resistivity structure of the lithosphere and the tectonic stabilisation-age of the terrane is evident. Good agreement between the inferred present-day lithospheric geotherms and surface heat flow measurements indicate the latter are strongly controlled by variations in lithospheric thickness. A significant difference in lithospheric thickness is observed between the Eastern and Western Kimberley blocks, and is consistent with previous seismic tomography images of the Kaapvaal Craton. The present-day lithospheric thickness, and reduced depth extent into the diamond stability field, accounts for the absence of diamondiferous kimberlites in the Gibeon and Gordonia kimberlite fields in the Rehoboth Terrane. Previously published mantle xenolith $P–T$ arrays from the Gibeon, Gordonia and Kimberley fields, however, suggest that the Rehoboth Terrane had equilibrated to a cooler conductive palaeo-geotherm (40–42 mW m$^{-2}$), very similar to that of Eastern Kim-

berley Block of the Kaapvaal Craton, at some time prior to the Mesozoic eruption of the kimberlites. The timing and nature of both the thermal equilibration of the Rehoboth Terrane, and the subsequent lithospheric heating/thinning event required to account for its present-day lithospheric structure, are not well constrained. A model consisting of the penetration of heat transporting magmas into the lithosphere, with associated chemical refertilisation, at an early stage of Mesozoic thermalism appears to be the most plausible model at present to account for both the present-day lithospheric structure of the Rehoboth Terrane and an earlier, cooler palaeogeotherm. Some problems, however, remain unresolved in terms of the isostatic response of the model. Based on a compilation of xenocryst Cr/Ca-in-pyrope barometry observations, the extent of depleted mantle in the Rehoboth Terrane is found to be significantly reduced with respect to the Eastern Kimberley Block: 117 km versus 138–167 km. It appears most likely that the depletion depth in both terranes, at least in the vicinity of kimberlite eruption, is explained by refertilisation of the lower lithospheric mantle.

© 2009 Published by Elsevier B.V.

## 1. Introduction

The Rehoboth Terrane (or Nama or Namibia Province) of southern Africa is accreted to the western margin of the Archaean Kaapvaal Craton (Fig. 1) and is largely hidden beneath thick Quaternary Kalahari sandcover. Current understanding of the nature of the Rehoboth lithosphere is based entirely on the analysis of mantle xenoliths found in kimberlites from the Gibeon and Gordonia kimberlite fields, located on the western margin of the terrane (Fig. 1). The lithospheric root of the Rehoboth Terrane has not been imaged before using geophysical methods, nor are there any reported surface heat-flow measurements for the terrane. While available geochemical and isotopic data, discussed later in the paper, point towards an early Proterozoic, rather than Archaean, affinity and age of stabilisation for the Rehoboth lithosphere, the lithospheric thickness, mantle geotherm and diamond prospectivity of the terrane are all subjects of ongoing debate, principally due to the paucity of data.

A large number of kimberlite pipes have been discovered within the Rehoboth Terrane, in the Gibeon and Gordonia fields (Fig. 1), but none are reported to be diamondiferous[4]. Early reports of the extensively prospected Rietfontein pipe in the Gordonia field (Fig. 1) referred to it as being diamondiferous (e.g., Gurney et al., 1971), but more recent discussions suggest that the pipe is, in fact, non-diamondiferous (Gurney, 1984; Dawson, 1989; Appleyard et al., 2007). The absence of diamondiferous kimberlites in the Gibeon and Gordonia areas suggests a lithospheric thickness not significantly greater than the depth of the graphite-diamond stability field, at least at the time of kimberlite eruption (75–65 Ma; Spriggs, 1988; Allsopp et al., 1989; Davies et al., 2001). The Tsabong kimberlite field (Fig. 1), located in the western-most Kaapvaal Craton, in the area of the Kheis Fold Belt immediately east of the Rehoboth Terrane, is reported as being diamondiferous by an exploration company active in the area, based on macro and microdiamond recoveries (http://www.firestonediamonds.com/tsabong). No mines are yet operating in the area.

In this paper we present a new deep lithospheric electrical-resistivity model, provided by 2-D magnetotellurics (MT), along a profile that crosses the Kaapvaal Craton, the Rehoboth Terrane and the Damara and Ghanzi-Chobe Belts (Fig. 1). The geophysical model, which shows significant lateral heterogeneity in the present-day lithospheric structure, is compared with the mantle geotherms predicted by peridotite xenolith pressure–temperature (P–T) arrays from the 140–70 Ma Kimberley and Gibeon kimberlite fields (Bell et al., 2003; Grütter and Moore, 2003; Boyd et al., 2004). The comparison provides new constraints on the lithospheric evolution of the terranes traversed, and also helps explain the absence of diamondiferous kimberlites in the Rehoboth Terrane. Comparison between the MT and xenolith data is complicated by the time and spatial sampling-scale differences between the present-day MT observations and the xenolith results that reflect the char-

acteristics of the lithosphere at the time of kimberlite eruption, or earlier. The latter data are also susceptible to thermal and/or chemical overprinting during the thermal event generating the eruption.

Magnetotellurics (MT) is a passive-source geophysical method used to derive electrical resistivity images of the subsurface. The method has been used widely in the investigation of lithospheric structure elsewhere in the world, for example in Canada (Jones et al., 2003), Europe (Korja, 2007) and Australia (Heinson and White, 2005). Magnetotellurics is an effective tool for investigating the thermal structure of the lithosphere, and hence lithospheric thickness, because the resistivity of the major mantle minerals (olivine, orthopyroxene and clinopyroxene) is highly sensitive to temperature variation (e.g., Constable et al., 1992; Xu and Shankland, 1999; Xu et al., 2000; Constable, 2006). For cratonic lithosphere, electrical resistivity is less sensitive to compositional variation in the mantle than is seismic velocity (Jones et al., 2009). Due to the close mapping between temperature and electrical resistivity in the mantle, lithospheric thickness is used throughout this paper, unless otherwise specified, in a "thermal" sense, i.e., the thickness defined by the intersection of a conductive mantle geotherm and the mantle adiabat.

## 2. Geological framework

MT profile KIM-NAM (Fig. 1) investigates a lithospheric accretionary history that was initiated during Palaeoarchaean times, with the first crustal formation and mantle melt depletion events recorded in the Kaapvaal Craton, and ended with the stabilisation of the Damara Mobile Belt following the Late Proterozoic/Early Palaeozoic Pan-African orogeny. The Kaapvaal Craton is subdivided into two tectonic blocks, the eastern Witwatersrand Block and the western Kimberley Block (de Wit et al., 1992), each with distinct geological fabrics and characteristics that attest to separate Palaeoarchaean to Mesoarchaean histories prior to their collision and accretion at about 2.9 Ga (Schmitz et al., 2004). The magnetic Colesberg Lineament (Fig. 1) defines the suture zone between the two blocks. Geological evidence, in the form of variations in magmatism and erosion levels on either side of the Colesberg Lineament, suggests that convergence between the two terranes was accommodated by subduction beneath the Kimberley Block (Schmitz et al., 2004).

A significant later tectonic event on the western margin of the Kaapvaal Craton resulted in the emplacement, from the west, of the thin-skinned Kheis Fold Belt (Fig. 1) onto the Kimberley Block sometime between 1.93 and 1.75 Ga (Tinker et al., 2004). Evidence presented later in the paper shows that the present-day lithospheric structure beneath the western part of the Kimberley Block, beneath the Kheis Fold Belt, is significantly different to that beneath the eastern part. The terms "Western Kimberley Block" and "Eastern Kimberley Block" are used throughout the text to refer to these two lithospheric blocks. Based on stratigraphic evidence in seismic reflection data, Tinker et al. (2004) and de Wit and Tinker (2004) interpret the presence of Ventersdorp Supergroup (2.70–2.65 Ga) stratigraphy across the entire Kimberley Block, including at depth below the Kheis Fold Belt. Whether the Western and Eastern Kimberley Blocks were ever separate entities is

---

[4] The terms "diamondiferous" and "non-diamondiferous" are used loosely in the paper, and reports that refer to kimberlites as being diamondiferous or not have been taken at face value. None of the databases, papers or websites referred to in this work quantify diamond grade in any way.
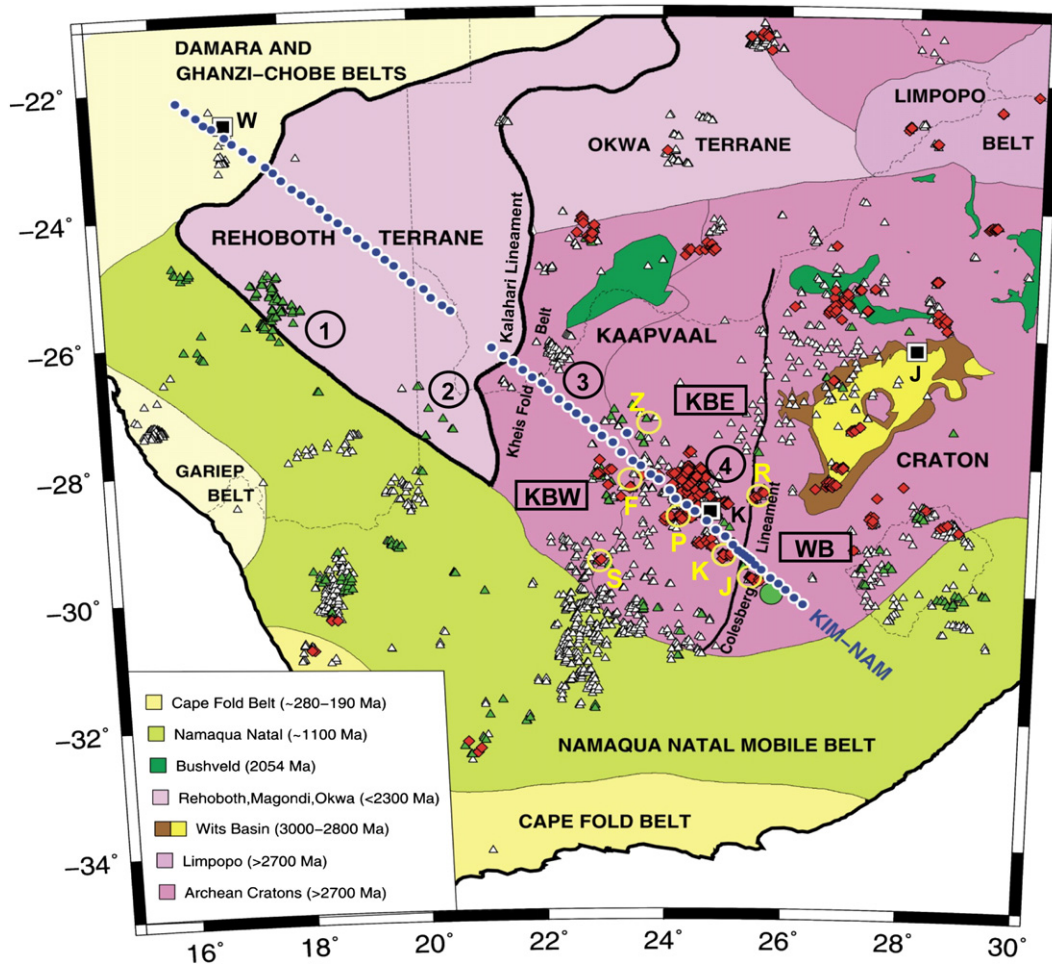
**Fig. 1.** Locality of MT profile KIM-NAM on simplified tectonic map of southern Africa. Shown are MT station sites (blue dots) and kimberlite occurrences (red diamonds = known diamondiferous, green triangles = known non-diamondiferous, white triangles = unknown or unspecified in databases). Annotated kimberlite fields are: (1) Gibeon, (2) Gordonia, (3) Tsabong and (4) Kimberley. Specific kimberlites referred to in Table 1 are shown by yellow circles: (J) Jagersfontein, (R) Roberts Victor, (K) Koffiefontein, (P) Paardeberg, (F) Finsch, (Z) Zero, (S) Sanddrift. Subdivision of Kaapvaal Craton into Western Kimberley Block (KBW), Eastern Kimberley Block (KBE) and Witwatersrand Block (WB) is shown. Green circle near Jagersfontein kimberlite shows location of the Trompsburg Igneous Intrusion. Major cities (black squares) are annotated: Kimberley (K), Johannesburg (J) and Windhoek (W). Sources of kimberlite data: South African Council for Geoscience numerical database; Jelsma et al. (2004); Faure (2006). Terrane boundaries shown courtesy S.J. Webb, University of the Witwatersrand, and based on the magnetic field image of southern Africa.

not known, but the distribution of Ventersdorp stratigraphy requires them to be a coherent tectonic unit by 2.7 Ga at the latest. The Rehoboth Terrane was accreted to the western margin of the Kimberley Block, across the magnetic Kalahari Lineament (Fig. 1), by about 1750 Ma (Jacobs et al., 2008).

The Rehoboth Terrane is recognised as a distinct tectonic unit most clearly in magnetic images of the subcontinent (see e.g., de Wit et al., 2004). The nature of the deeper crust is obscured by extensive Late Cretaceous to Recent Kalahari sediments and sand-cover (Haddon, 2005), and by relatively undeformed Carboniferous to Cretaceous Karoo (e.g., Wanke, 2000) and Late Proterozoic/Early Phanerozoic Nama stratigraphy (Hartnady et al., 1985). These younger sequences are known to be underlain by the, at least, 5 km thick volcano-sedimentary Rehoboth Group (Becker et al., 2004), a volcanic component of which has been dated at $1782 \pm 10$ Ma (zircon U–Pb age, Nagel et al., 1996). Several key observations indicate an Early Proterozoic stabilisation age for the Rehoboth lithosphere. The oldest Rehoboth crustal ages yet identified are between 2.3 and 1.7 Ga (Nd model and zircon $^{207}Pb/^{206}Pb$ ages, Ziegler and Stoessel, 1991) for the Weener Intrusive Suite on the northern margin of the terrane. Mantle peridotite xenoliths from the Gibeon kimberlite field provide model Re depletion ages (indicating the age of partial melt extraction from the mantle) of between 2.2 and $2.0 \pm 0.2$ Ga (Hoal et al., 1995), which are ~1 Ga younger than the

oldest Re depletion ages observed on the Kaapvaal Craton (Boyd et al., 2004). No Archaean ages have yet been reported for any Rehoboth crustal or mantle samples.

Renewed tectonic activity after a 350 Ma quiescent period, reworking of old Palaeoproterozoic units and growth of new lithospheric material during the Mid to Late Mesoproterozoic resulted in the collision and emplacement of the Namaqua–Natal Mobile Belt (Fig. 1) along the southwestern margins of both the Kaapvaal Craton and Rehoboth Terrane (Jacobs et al., 2008). The 7 km thick, largely undeformed, volcano-sedimentary Koras Group, dated at $1171 \pm 7$ Ma (Gutzmer et al., 2000), is observed to unconformably overly both the Kheis and Namaqua belts (Jacobs et al., 2008), and provides an age bracket for the end of the Namaqua orogeny.

Following the termination of the Namaqua orogeny, Neoproterozoic rifting along the northwestern margin of the Rehoboth Terrane resulted in the deposition of the largely sedimentary units that make up the earlier Ghanzi-Chobe (Modie, 2000) and the later Damara successions (Jacobs et al., 2008). The Damara rift system was active between at least 900 and 750 Ma (Jacobs et al., 2008). Tectonic inversion and deformation of the rift successions, by folding and thrusting, followed during the Late Neoproterozoic/Early Palaeozoic "Pan African" Damara orogeny (Modie, 2000; Jacobs et al., 2008). The Nama Group referred to above, with basal units dated between ~550 and 540 Ma,

and overlying much of the Rehoboth Terrane, is interpreted as the foreland basin succession to the Damara orogen (Prave, 1996). Given the lithospheric scale of investigation of the MT profile, the Ghanzi-Chobe Belt and Damara Belt are not differentiated, and are referred to as the "Ghanzi-Chobe/Damara Belt" for simplicity throughout the paper.

Subsequent to the stabilisation of the Damara Belt at the end of Pan-African tectonism, the subcontinent was exposed to the thermalism associated with the Jurassic breakup of Gondwana and the Cretaceous thermal event that generated most of the kimberlites found in the vicinity of the MT profile (Fig. 1). The bulk of the kimberlites in the Kimberley area are aged between 143 and 117 Ma (Group 2 kimberlites) or 108 and 74 Ma (Group 1 kimberlites) (Griffin et al., 2003; Kobussen et al., 2008). The Rietfontein pipe in the Gordonia field (Fig. 1) is a Group 1 type kimberlite (Appleyard et al., 2007) and has been dated at between 71.9 and 71.1 Ma (zircon U–Pb age, Davis et al., 1976). Kimberlites in the Gibeon field (Fig. 1) have been dated between 75 and 65 Ma (Spriggs, 1988; Allsopp et al., 1989; Davies et al., 2001).

## 3. Magnetotellurics

### 3.1. Data acquisition and processing

The magnetotelluric method records, at stations located on the Earth's surface, the subsurface electrical field variations that are induced by the natural time-variation in the Earth's magnetic field strength. The measured electrical and magnetic field variations are used to derive the "MT response" (the impedance tensor) at each observation site, which is subsequently numerically modelled to derive an image of the subsurface electrical-resistivity structure (Simpson and Bahr, 2005, provide a useful introductory text to the MT method). In the case of 2-D subsurface electrical-resistivity structure, two mutually orthogonal electrical fields propagate through the Earth. The transverse-electrical (TE) mode propagates parallel to the electrical strike direction, while the transverse-magnetic (TM) mode propagates perpendicular to electrical strike. The electrical strike direction is controlled by the strike of the geological structures and by the alignment of minerals. Both TM and TE mode data in the measured MT response are modelled simultaneously in developing a 2-D electrical-resistivity model of the subsurface. Practical problems in deriving 2-D models, due to the electrical distortion of the MT response and the fact that subsurface geology may consist of 3-D structures, are addressed below.

MT data were acquired at 69 broadband stations (data periods ~0.003–5,000 s), deployed at roughly 20 km intervals along the KIM-NAM profile (Fig. 1), recording data for two- or three-night periods. Additionally, 10 coincident long-period stations (~10–10,000 s) were deployed at roughly 60 km intervals along the southern portion of the profile, recording data for approximately one-month periods. Data acquisition took place during the first and last quarters of 2004 as part of the larger Southern African MT Experiment (SAMTEX) (Jones et al., this issue). The instrumentation consisted of Phoenix MTU5 broadband and LIMS long-period units. The gap in station coverage, towards the midpoint of the profile, is due to the lack of access inside the Kgalagadi Transfrontier National Park located in southwestern Botswana.

Three different robust processing codes using remote referencing methods (those of Jones, Egbert and Chave, see Jones et al., 1989, methods 6, 7 and 8 respectively therein) were tested and used at different stations along the profile to derive optimal MT responses. While data

quality across the Rehoboth Terrane is good, very poor data quality prevails within a radius of about 100 km around the town of Kimberley, due to the high amplitude electrical-noise generated by the DC power-supply to both the mines and railway lines located in the area.

### 3.2. Geoelectric strike direction and data decomposition

The process of MT data decomposition is required to determine, at each individual MT site, (i) the 2-D geoelectric strike direction, and (ii) whether the MT data are suitable for 2-D modelling along a profile. If the MT site responses are not adequately two-dimensional in character (i.e., they are closer to 3-D), they cannot be modelled validly using a 2-D approach. Decomposition also removes local-scale galvanic (electrical) distortion from the MT site responses that might otherwise obscure the regional 2-D geological response (Groom and Bailey, 1989). Once the best electrical strike direction is determined, the MT responses at each site are modelled in that coordinate system.
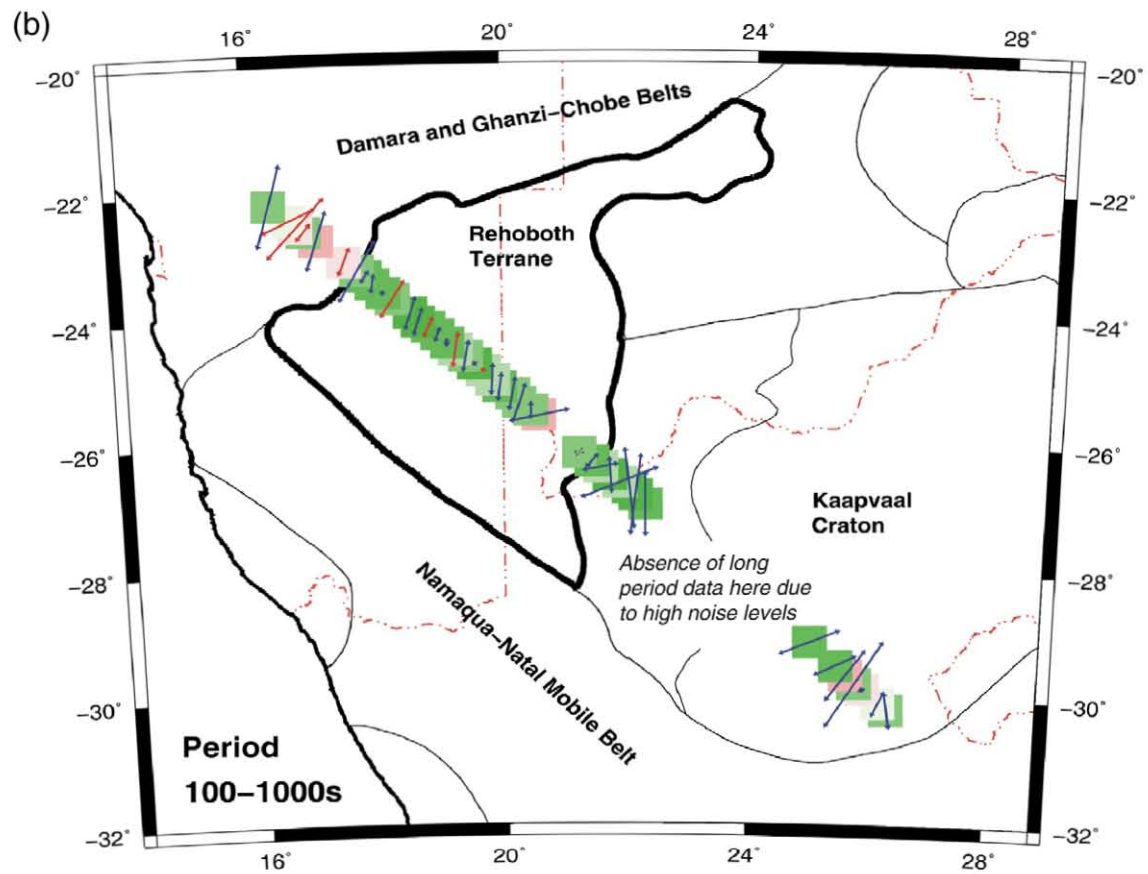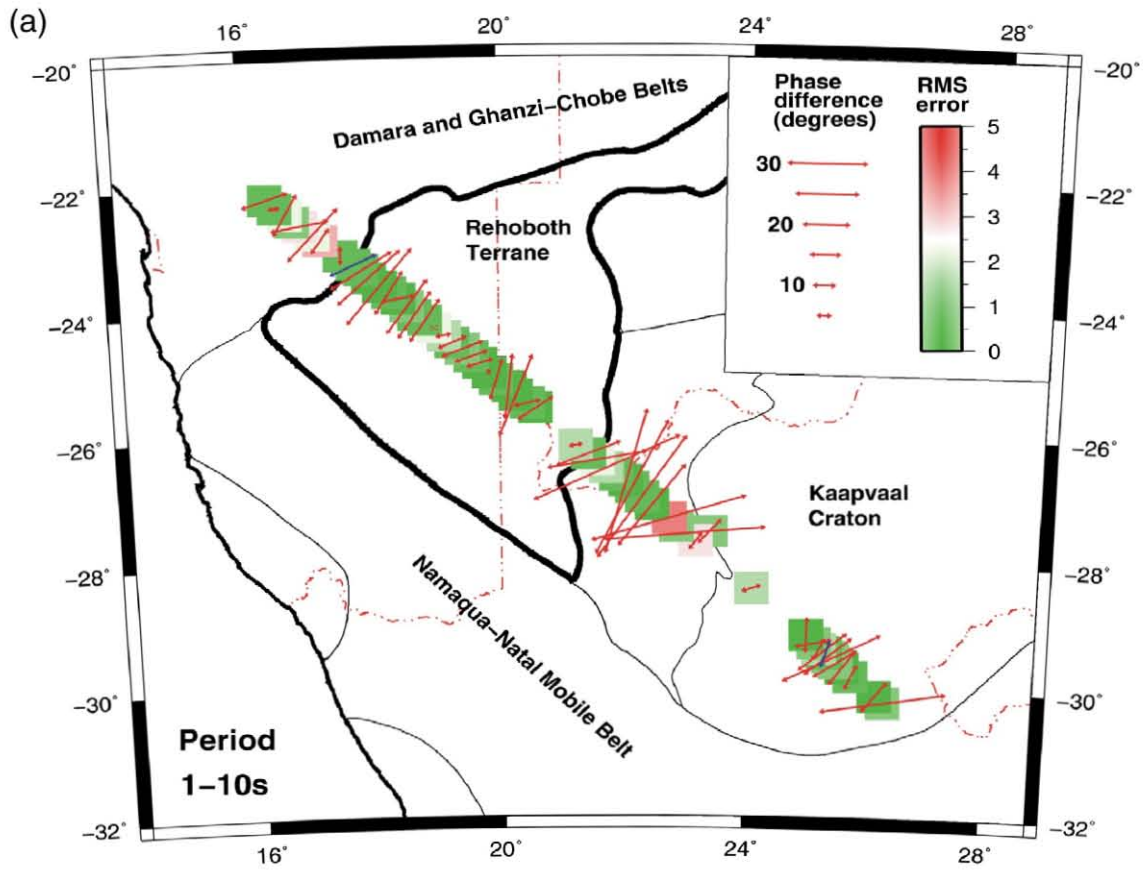
MT data at each site were decomposed using the method of Groom and Bailey (1989), as implemented in the STRIKE code of McNeice and Jones (2001). The Groom and Bailey decomposition method models simultaneously the best 2-D electrical strike direction and a set of electrical "distortion parameters" for each site. The results of the decomposition (Fig. 2) confirm that 94% of the MT responses along the profile are consistent with a 2-D assumption (i.e., the decomposition-model RMS errors are small — see Fig. 2 caption), and are therefore suitable for 2-D modelling. Electrical strike direction is observed to vary from terrane to terrane. Consistent strike directions in the range 5–25° E of N are observed within the mantle lithosphere of the Rehoboth Terrane (Fig. 2b). A strike of direction of closer to 45° E of N is indicated for both the Damara Belt and Kaapvaal Craton (Fig. 2a and b). In principle, four or five adjacent MT sites sample the same subsurface lithospheric volume at depth and should return the same regional electrical strike direction. In practice, however, some station-to-station variability emerges because of local-scale 3-D structure, which can vary significantly from site-to-site.

Two-dimensional MT modelling and inversion codes make the implicit assumption that the electrical strike direction is constant along the entire profile. To accommodate the variable geoelectric strike observed along profile KIM-NAM within the limitations imposed by 2-D modelling, two strike directions, 25° and 45°, were chosen for the decomposition of the MT responses, and these two datasets were subsequently modelled separately and independently. The problem of variable electrical strike direction can, in principle, be dealt with fully by using a 3-D modelling approach. Academic codes that perform 3-D modelling are, however, not yet mature enough to accommodate a large number of MT sites together with an adequately discretised subsurface model mesh.

### 3.3. 2-D electrical resistivity modelling

2-D electrical resistivity models of the subsurface (Fig. 3) were computed by 2-D simultaneous smooth inversion of all the MT responses along the profile, independently for both 25° and 45° strike directions. The inversion method used is that of Rodi and Mackie (2001), and the inversion parameters used are specified in the caption to Fig. 3. The smoothness of the models was controlled in the inversion to produce the "minimum-structure" models required to satisfy the observed MT responses.

**Fig. 2.** Results of MT strike analysis along profile KIM-NAM using Groom and Bailey (1989) decomposition. (a.) Data period 1–10 s (mostly crustal depths) and (b.) data period 100–1000 s (mostly upper to lower lithospheric-mantle depths). Double-headed vectors show 2-D geoelectrical strike direction, scaled in length by phase difference between the TM and TE modes, and colour coded by depth of penetration (red<50 km, and blue>50 km). A large phase difference indicates strongly 2-D, rather than 1-D, structure. Coloured squares show the RMS misfit error, normalised by the observational errors in the observed MT response, at each site. The RMS (root-mean-square) error is the difference between the observed MT response and the MT response of the 2-D decomposition model (consisting of the best electrical strike direction and several distortion parameters). By normalising the RMS error by observational errors, higher quality data with low errors are weighted more heavily in the decomposition. Low RMS errors (<~2) indicate MT responses in which the subsurface structure is adequately described as 2-D, rather than 3-D, and which are free of galvanic distortion.

(a) Period 1–10s

(b) Period 100–1000s

Absence of long period data here due to high noise levels

Phase difference (degrees)

RMS error

Damara and Ghanzi–Chobe Belts

Rehoboth Terrane

Kaapvaal Craton
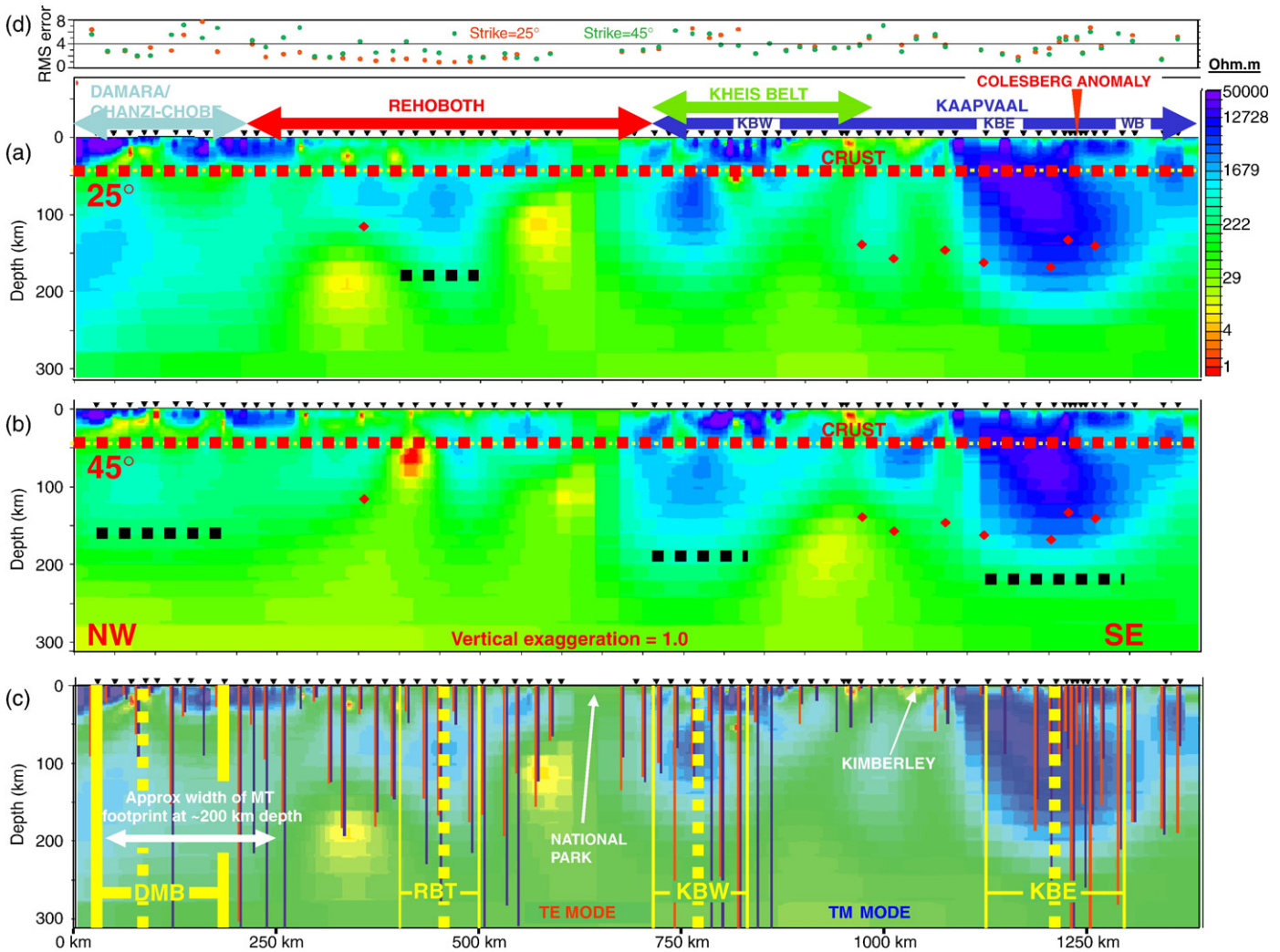
Namaqua–Natal Mobile Belt

Fig. 3. Electrical resistivity models for profile KIM-NAM derived from 2-D smooth inversion of decomposed MT station responses for (a.) 25° E of N strike azimuth and (b.) 45° E of N azimuth. (c.) Estimates of the depth of penetration achieved at each individual station location for both the TE (red) and TM (blue) modes, and overlaid on the 25° inversion model. The models are entirely unconstrained (and should be ignored) in areas beneath the maximum depth of penetration. (d.) 2-D inversion RMS misfit error at each station. The surface extent of the geological terranes is shown in (a.) and abbreviations used as follows: Ghanzi-Chobe/Damara (DMB), Rehoboth (RBT), Western Kimberley Block (KBW), Eastern Kimberley Block (KBE) and Witwatersrand Block (WB). Black dashed lines in (a.) and (b.) indicate interpreted depth to base of lithosphere, where well constrained, and red diamonds indicate the depth to the base of the chemically depleted lithosphere as defined by Cr/Ca-in-pyrope barometry from kimberlitic concentrates (Table 1). The solid vertical yellow lines in figure (c.) define the zones used in each terrane to compute the average resistivity profiles presented in Fig. 4 (using the 25° model for RBT, and the 45° model for DMB, KBW and KBE). The dotted vertical yellow line in each terrane in figure (c.) shows the position of the "maximum" resistivity profile in Fig. 4 (using the same strike azimuth models as for the average profiles). The 2-D inversion method used is that of Rodi and Mackie (2001) implemented in WinGLink® software. Inversion parameters used as follows: simultaneous inversion for phase and apparent resistivity for both TE and TM modes, and for static shift, with smoothing factor $\tau = 3.0$ and error-floors for phase and apparent resistivity set to 5% and 10% respectively. Tipper (Hz) data, although available at some stations, were not used. The value of the parameter controlling the smoothness of the model, $\tau$, was chosen based on an L-curve test of model RMS error versus $\tau$. Increasing the value of $\tau$ above the chosen value of 3.0 (i.e., increasing the spatial complexity of the model) provided no significant improvement in the model RMS error, and the final models represent the "minimum-structure" models required to satisfy the observed MT responses. The depth of penetration is calculated using a 1-D Niblett–Bostick inversion (Jones, 1983). The 2-D inversion RMS misfit errors are the root-mean-square differences between the observed and calculated MT responses at each site, normalised by the MT data errors (which include both "observational" and "2-D decomposition" errors). By normalising the RMS error by MT data errors, higher quality data with low errors are weighted more heavily in the inversion. Furthermore, because "decomposition" errors are incorporated into the MT data error, the final 2-D models only match the MT data observations to the extent to which they are two-dimensional.

Depth of penetration along the profile (Fig. 3c) is variable and is dependent on both the subsurface electrical conductivity (the inverse of resistivity) and the maximum reliable period recorded in the data at each site. Long-period (low-frequency) data provide greater depths of penetration, while high subsurface conductivities restrict the depth of penetration. With the exception of the areas around Kimberley (industrial noise problems) and beneath the Kgalagadi Transfrontier National Park (no data coverage), depths of penetration to about 200 km have been achieved everywhere in the models, and up to depths closer to 300 km beneath the more resistive areas, in at least one of the two MT modes. Generally the MT method samples, below each MT station, a "footprint" or "hemisphere of influence" with a diam-

eter roughly equal to the depth of investigation. At a 200 km depth, for example, the MT footprint would need to be sampled at approximately 100 km intervals to provide adequate spatial sampling. It is evident in Fig. 3c that the deep subsurface is adequately sampled with respect to the size of the footprint everywhere in the model except for the two areas mentioned above, where the subsurface is not constrained in any way.

Features in the MT subsurface models are variably sensitive to the choice of strike direction over the 25°–45° range (Fig. 3a and b), and it is important to examine the structure in each terrane with reference to its appropriate electrical strike direction, i.e., 25° for the Rehoboth Terrane, and 45° for the Kaapvaal Craton and the Ghanzi-Chobe/Damara

Belt. There is some variation apparent in the positioning of the conductive anomalies in the subsurface when comparing the two different strike directions, and these features are considered to be less reliably defined than the first-order features — the resistive lithospheric roots — which are regarded as robust and reliably defined. Imaging of the Rehoboth Terrane lithosphere in particular is improved in the 25° strike model, corresponding with a noticeable improvement in the RMS model misfit error (Fig. 3d).

### 3.4. Interpretation of 2-D electrical resistivity models

Significant heterogeneity is observed in the thickness and resistivity of the lithospheric mantle along the profile. The Kaapvaal Craton imaged on the southeastern end of the profile (the Eastern Kimberley Block) is characterised by very thick, very resistive lithosphere. In contrast, the lithosphere beneath the Kaapvaal Craton in the vicinity of the Kheis Fold Belt (the Western Kimberley Block), and beneath the Rehoboth Terrane, is significantly thinner and less resistive. Further northwest, the lithosphere beneath the Ghanzi-Chobe/Damara Belts is characterised by the thinnest and most conductive lithosphere along the profile. In the analysis that follows we focus specifically on those parts of the models that are, firstly, best constrained geophysically and secondly, correspond with the thickest, most resistive lithospheric sections that are the most prospective for diamonds. The thickness of resistive features is well constrained by the MT method (Jones, 1999), and therefore allows a reliable estimate to be made of lithospheric thickness in the areas selected for analysis. In attempting to account for the occurrence of non-diamondiferous kimberlites in the Rehoboth Terrane, if the maximum lithospheric thickness proves insufficient to provide deep penetration into the diamond stability field, then the same will be true for thinner lithosphere.

Curves of average and maximum resistivity versus depth for each terrane (Fig. 4), calculated within the areas defined in Fig. 3c using the 25° strike model (Fig. 3a) for the Rehoboth Terrane and the 45° strike model (Fig. 3b) for all the other terranes, illustrate clear differences in the bulk resistivity characteristics of each terrane traversed. For example, at a depth of 100 km the average resistivity of the Eastern Kimberley Block is ~10,000 Ω m, while that of the Rehoboth Terrane is ~1000 Ω m, an order of magnitude less, and that of the Ghanzi-Chobe/Damara Belt is ~500 Ω m (note that the abscissa scale in Fig. 4 is log resistivity). As the electrical resistivity of mantle minerals decreases strongly with increasing temperature (Constable et al., 1992; Xu and Shankland, 1999; Xu et al., 2000), hotter geotherms, associated with thinner lithosphere, result in lower bulk mantle resistivities (Fig. 4). Electrical resistivity is significantly less sensitive to compositional variation in the mantle than it is to temperature (Maumus et al., 2005; Jones et al., 2009). The differences observed in the bulk resistivities of each of the terranes traversed are therefore most readily accounted for by variations in the temperature of the lithosphere, i.e., the lithospheric geotherm. Along profile KIM-NAM, the coolest geotherm (and thickest lithosphere) is therefore associated with the Eastern Kimberley Block, and the hottest geotherm (and thinnest lithosphere) with the Ghanzi-Chobe/Damara Belt.

The observed resistivity-depth profiles in Fig. 4 systematically fail to match the very high resistivities predicted in the upper mantle for dry cratonic lithosphere above about 120 km depth. Several possible reasons could account for the failure: (i) while the MT method is sensitive to the thickness of resistive layers, it has a relatively low sensitivity to their resistivity, particularly when the resistive layer is located below a more conductive layer such as the crust (see, e.g., Jones, 1999), (ii) the regularisation (smoothing) inherent in the 2-D smooth inversion algorithm used, as well as the averaging used to compute the depth profiles (although the profile variance is very small at lithospheric depths), and (iii) there may be other properties systematically affecting electrical conductivity that are not accounted for in the temperature-based model used, for example the presence of hydrogen in
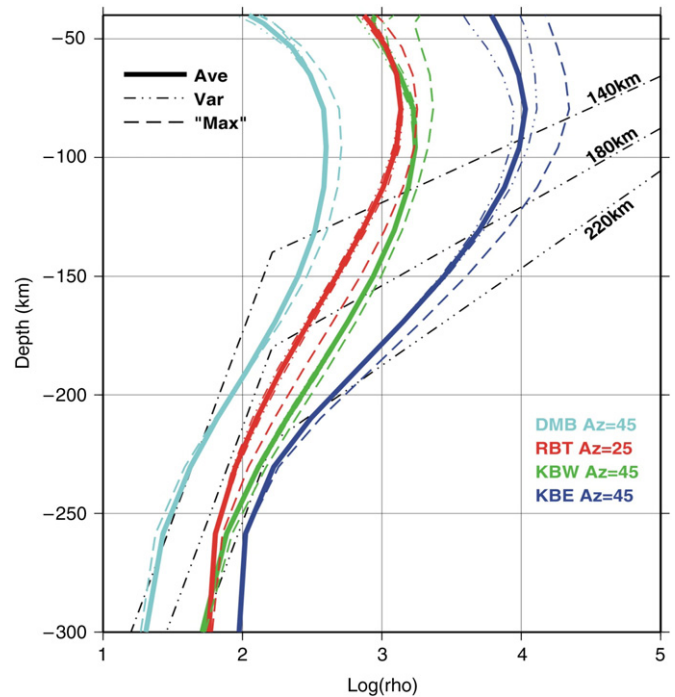


Fig. 4. Electrical resistivity versus depth profiles for geological terranes traversed by profile KIM-NAM. Profiles of average resistivity, variance, and "maximum" resistivity are shown as indicted in the key. The average (and variance) profiles are computed from the 2-D sections of Fig. 3a (for RBT only) and Fig. 3b (for DMB, KBW and KBE), within the spatial areas defined in Fig. 3c. The "maximum" resistivity profiles are single illustrative profiles extracted from the models at the positions indicated in Fig. 3c, in the vicinity of highest resistivity values in the lithospheric depth range 50–150 km (using the same strike azimuth models as for the average profiles). Predicted resistivity-depth profiles for hypothetical mantle geotherms for different lithospheric thicknesses are shown (black dotted and dashed lines), based on laboratory electrical-conductivity versus temperature and pressure measurements for dry olivine and pyroxene (Constable et al., 1992; Xu and Shankland, 1999; Xu et al., 2000). The inflection point in the theoretical curves corresponds with the intersection of the conductive mantle geotherm with the adiabat. Terrane code names as for Fig. 3.

the mantle (Karato, 1990, 2006). Nevertheless, the *relative* variation in average resistivity from terrane to terrane is reliably defined.

As the 2-D inversion models and the resistivity-depth profiles derived from them are smooth, the transition from the lithosphere into the more electrically conductive mantle asthenosphere below is not sharply defined. *Relative* lithospheric thickness variations between each terrane can, however, be determined from the observed systematic changes in bulk resistivity. Providing a useful frame of reference is the observation, in the theoretical curves of Fig. 4, that an order of magnitude difference in electrical resistivity in the depth range 100–150 km can be accounted for by a ~40 km lithospheric thickness change. With respect to the observed resistivity-depth profile of the Eastern Kimberley Block in Fig. 4, the Western Kimberley Block is interpreted to be associated with ~30 km thinner lithosphere, the Rehoboth Terrane with ~40 km thinner lithosphere, and the Ghanzi-Chobe/Damara Belt with ~60 km thinner lithosphere. An *absolute* depth to the base of the lithosphere cannot reasonably be inferred deeper than ~250 km in the Eastern Kimberley Block (Figs. 3b and 4), and a depth close to ~220 km is regarded as the most reasonable estimate. Absolute depths to the base of the lithosphere are therefore inferred to be 190 km, 180 km and 160 km for the Western Kimberley Block, the Rehoboth Terrane and the Ghanzi-Chobe/Damara Belt respectively (Fig. 3a and b). Given that the vertical cell dimension is about 20 km at a depth of 200 km in the models, the depth of the lithosphere–asthenosphere boundary cannot be identified to a precision of better than about ±20 km.

## 4. Xenolith geochemistry and thermobarometry

### 4.1. Lithospheric mantle depletion

Available evidence from xenolith studies indicates that the lithospheric mantle of the Rehoboth Terrane is chemically less depleted on average, reflecting lower degrees of partial melting, and has a thinner highly-depleted upper lithospheric mantle layer, in comparison with the Eastern Kimberley Block of the Kaapvaal Craton. Low-temperature peridotites from the Gibeon field have an average Mg# for olivine equal to 91.6 in comparison with 92.6 for the Kaapvaal Craton (Boyd et al., 2004). Grütter et al. (1999, 2006) have used Cr saturation in garnet xenocrysts from kimberlites to define the maximum pressure (and therefore depth) of depleted peridotite in the mantle. Such maximum-pressure estimates from Cr-rich garnets from several southern African kimberlites (Table 1 and Fig. 3) indicate that the chemically depleted lithosphere extends significantly deeper beneath the Eastern Kimberley Block than beneath the Rehoboth Terrane: 138–167 km versus 117 km respectively, assuming a pressure-depth conversion factor of 3 km/kbar. The maximum-pressure estimates are only moderately sensitive to the geotherm assumed (38 mW m$^{-2}$) in their calculation. Increasing the geotherm by 2 mW m$^{-2}$ has the effect of decreasing the maximum-pressure by less than 1 kbar.

Within the Eastern Kimberley Block, the depth extent of the highly-depleted upper lithospheric mantle appears to be defined by refertilisation of the underlying lithosphere that took place between the eruption of Group 2 kimberlites (143–117 Ma) and Group 1 kimberlites (108–74 Ma) (Griffin et al., 2003; Kobussen et al., 2008). The vertical extent of the depleted upper lithospheric mantle, expressed by the presence of low-Ti in garnet xenocrysts, decreased from ~190 km to ~150 km between the eruptions of the two groups of kimberlites (Kobussen et al., 2008). Maximum-pressure estimates from Cr-rich garnets (Table 1) are in accord with these observations: kimberlites older than 120 Ma define a maximum depletion depth close to 170 km, while the maximum depth defined by the two kimberlites erupted after 90 Ma is 145 km.

A significantly less depleted character for the Rehoboth lithosphere is indicated by the high percentage (60–75%) of "fertile lherzolites" mapped throughout the depth range 90–150 km in a "Namaqua" lithospheric section (Griffin et al., 2003, based on the compositions of kimberlitic Cr-pyrope garnet concentrates). The "Namaqua" section is felt to be representative of the Rehoboth Terrane as 75% of the "Namaqua" garnet samples are derived from kimberlites in the Gibeon and Gordonia kimberlite fields. In the Namaqua section, the percentage of depleted peridotite in the lithosphere peaks at ~40% in the depth range 95–115 km, falling off to ~15% at greater depths, and is consistent with the ~120 km maximum depth of depletion indicated by Cr-saturation in garnet xenocrysts (Table 1). Some of the garnet samples included in the "fertile lherzolite" category of Griffin et al. (2003) show evidence of metasomatism (both Fe and Ca–Al), indicating that the fertile character of the Rehoboth lithosphere may be due, in some part, to later refertilisation.



**Fig. 5.** Peridotite xenolith *P–T* arrays for the Gibeon, Kimberley and Northern Lesotho kimberlite fields. Temperatures calculated using the thermometer of Nimis and Taylor (2000) and pressures using the barometer NG85 (Nickel and Green, 1985). Model conductive geotherms (thin black lines, 35 to 50 mW m$^{-2}$) are after Pollack and Chapman (1977), terminating at a mantle adiabat with potential temperature $T_P$ = 1300 °C. The graphite/diamond equilibrium (thick black line) is that of Kennedy and Kennedy (1976). Gibeon localities: Anis Kubub, Gibeon Townlands, Hanaus and Louwrencia (dated 65–75 Ma, Spriggs, 1988 and Allsopp et al., 1989). Kimberley localities: De Beers, Bultfontein, Wesselton and Bultfontein Floors (dated 84 Ma, Allsopp and Barrett, 1975). Northern Lesotho localities: Letseng la Terae, Thaba Putsoa, Mothae, Matsoku, Kao, Liqhobong, Sekameng, Lemphane and Pipe 200 (dated ~90 Ma, Davis, 1977). References for geochemistry of xenolith samples are given in Appendix A.

### 4.2. Thermobarometry

Mantle xenolith pressure–temperature (*P–T*) arrays from the Kimberley and Gibeon kimberlite fields help constrain lithospheric mantle geotherms and lithospheric thickness at time of kimberlite eruption between ~140 and 70 Ma. Several studies have been published in which Gibeon peridotite arrays are either compared directly with equivalents from the Kimberley field (Bell et al., 2003; Grütter and Moore, 2003) (see Fig. 5) or are compared with the "Kalahari geotherm" of Rudnick and Nyblade (1999) (Boyd et al., 2004). The Kalahari geotherm is similar to the often used cratonic 40 mW m$^{-2}$ geotherm of Pollack and Chapman (1977) above ~120 km depth, but below 120 km the latter is hotter due to an assumption of greater heat production below 120 km (Boyd et al., 2004). In other recent work, the *P–T* array of orthopyroxene-bearing eclogites from the Rietfontein pipe in the Gordonia field of the Rehoboth Terrane has been compared with the Kalahari geotherm (Appleyard et al., 2007). All of these studies have used various combinations of the MC74 (MacGregor, 1974), NG85 (Nickel and Green, 1985), BKN90 (Brey et al., 1990) and NT00 (Nimis and Taylor, 2000) pyroxene-garnet thermobarometers. Results in which the Gibeon and Kimberley

**Table 1**
Maximum-pressure estimates for Cr-rich garnets in concentrate from kimberlites, derived using the Cr/Ca-in-pyrope barometer of Grütter et al. (2006).

| Kimberlite/cluster/group | Terrane/Block | Age (Ma) | Garnet count | Garnet Cr$_2$O$_3$ | Garnet CaO | $P_{38}$ (kbar) | Depth (km) | Reference |
|---|---|---|---|---|---|---|---|---|
| Jagersfontein | WB | 86 | 895 | 6.89 | 0.25 | 48.3 | 145 | Grütter et al. (2006, Fig. 8) |
| Roberts Victor | WB | 127 | 1587 | 9.52 | 0.62 | 55.7 | 167 | Grütter et al. (2006, Table 2) |
| Koffiefontein | KBE | 90 | 1003 | 6.77 | 0.93 | 45.9 | 138 | Grütter et al. (2006, Fig. 9) |
| Paardeberg | KBE | 120 | ~2500 | 10.18 | 1.44 | 55.3 | 166 | Grütter et al. (1999, Fig. 4d) |
| Finsch | KBE | 118 | 664 | 13 | 5.36 | 52.5 | 158 | Grütter et al. (2006, Fig. 7) |
| Zero | KBE | 1600 | ~300 | 9.72 | 2.77 | 49.8 | 149 | Grütter et al. (2006, Table 3) |
| Sanddrift | KBE | 126 | ~2500 | 8.2 | 1.54 | 48.5 | 146 | Grütter et al. (1999, Fig. 4c) |
| Gibeon | RBT | 70 | 2558 | 8.99 | 5.54 | 39.6 | 119 | Grütter et al. (1999, Fig. 1b) |

Age for the Paardeberg group is approximate. Garnet count is the total number of samples analysed at each pipe/cluster. $P_{38}$ is the maximum-pressure for an assumed 38 mW m$^{-2}$ geotherm. Depth is calculated from pressure using a 3 km/kbar conversion factor. KBE = Eastern Kimberley Block and WB = Witwatersrand Block of the Kaapvaal Craton. RBT = Rehoboth Terrane.
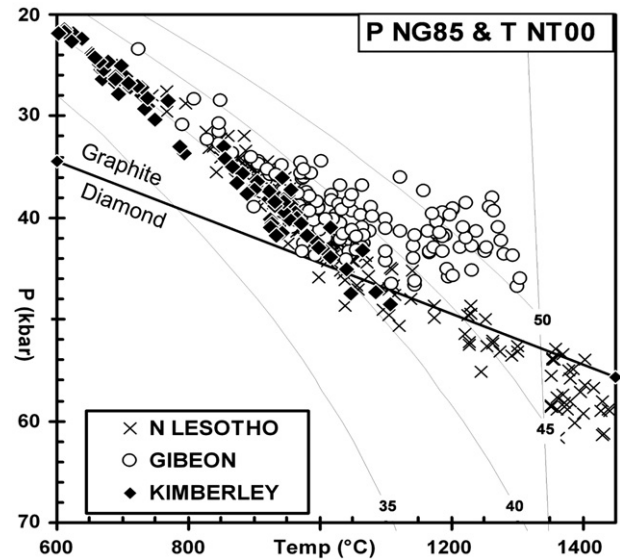
xenoliths are compared using the MC74 barometer are suspect: MC74 does not include Fe in its formulation, and therefore fails to account for the lower depletion levels, and higher Fe content, of the Gibeon peridotite xenoliths with respect to those from the Kimberley field.

The conclusion that has emerged from these studies is that, on balance, the Rehoboth Terrane and Eastern Kimberley Block had acquired similar thermal structures, defined by a conductive geotherm of about 40–42 mW m$^{-2}$ (Bell et al., 2003; Boyd et al., 2004; Appleyard et al., 2007), at some stage prior to kimberlite eruption. Geotherms of 40–42 mW m$^{-2}$ correspond with a thermal thickness of the lithosphere (defined by the intersection of the geotherm with the mantle adiabat) of between about 225 and 205 km. However, the evidence of disruption of the Gibeon array data at high temperatures (Fig. 5) suggests that the Rehoboth lithosphere subsequently experienced thermal perturbation either at, or sometime before, the time of kimberlite eruption (Bell et al., 2003). Sleep (2003) has shown that both the thermal influence of a plume and metasomatism are able to account for the high-temperature perturbation or "inflection" (Finnerty, 1989) that is observed in many P–T arrays worldwide, including the Gibeon array.

The Eastern Kimberley Block palaeo-geotherm is observed to have heated up from about 35 mW m$^{-2}$ to 37–38 mW m$^{-2}$ in the course of the thermalism, referred to above, that took place between the eruption of Group 2 and Group 1 kimberlites (Griffin et al., 2003). It is worth noting that the Kimberley P–T array in Fig. 5, defined by kimberlite eruptions from the period ~84 Ma, records the later, warmer geotherm (although the Fig. 5 data suggest a somewhat warmer geotherm of ~41 mW m$^{-2}$). The evidence suggests that it is possible to alter the lithospheric geotherm, at least in the region of kimberlite magmatism, over quite short periods of time, particularly where there is advection of heat by melts. The upper limit on the time period available to effect the observed change in the Eastern Kimberley Block geotherm is ~70 million years, the maximum time span between Group 2 and Group 1 eruptions.

## 5. Discussion

Given temperature as the primary control on the resistivity of mantle minerals, and that the MT derived lithospheric thickness therefore provides a reasonable proxy for the "thermal" thickness of the lithosphere (the thickness defined by the intersection of a conductive geotherm with the mantle adiabat), it is possible to determine approximate average present-day geotherms for each of the terranes traversed. Estimates of the geotherms, based on Pollack and Chapman (1977), are as follows (Fig. 6): 41 mW m$^{-2}$, 44 mW m$^{-2}$, 45 mW m$^{-2}$ and 48 mW m$^{-2}$ for the Eastern Kimberley Block, Western Kimberley Block, Rehoboth Terrane and Ghanzi-Chobe/Damara Belt respectively. That the Ghanzi-Chobe/Damara Belt area might be associated with hot (thin) lithosphere is supported by the very-high average surface heat-flow measurements recorded there in the vicinity of profile KIM-NAM: 69 mW m$^{-2}$ (1σ = 11 mW m$^{-2}$) for the Damara Belt and 63 mW m$^{-2}$ (1σ = 6 mW m$^{-2}$) for the Ghanzi-Chobe Belt (Jones, 1998). Hot mantle palaeo-geotherms, between 50 and 90 mW m$^{-2}$, are also indicated in P–T estimates of peridotitic xenolith samples from the Swakopmund (Whitehead et al., 2002) and Okenyenya (Baumgartner et al., 2000) alkali intrusions, both dated at ~75 Ma and located in the Damara Mobile Belt (outside the boundaries of Fig. 1, but both within ~200 km of the northwestern end of profile KIM-NAM). A low average surface heat flow value of 38 mW m$^{-2}$ (1σ = 7 mW m$^{-2}$) is reported for the "Western Sector" of the Kaapvaal Craton (Jones, 1998), and is in accord with the cool geotherm inferred from the MT model for the Eastern Kimberley Block. The similarity between the present-day geotherm and the xenolith derived palaeo-geotherm from the Kimberley field (Section 4.1) provides strong evidence that the thermal structure of the Eastern Kimberley Block has remained largely unchanged between the time of the eruption of the Group 1 kimberlites (~84 Ma, Allsopp and Barrett, 1975) and the present-day.
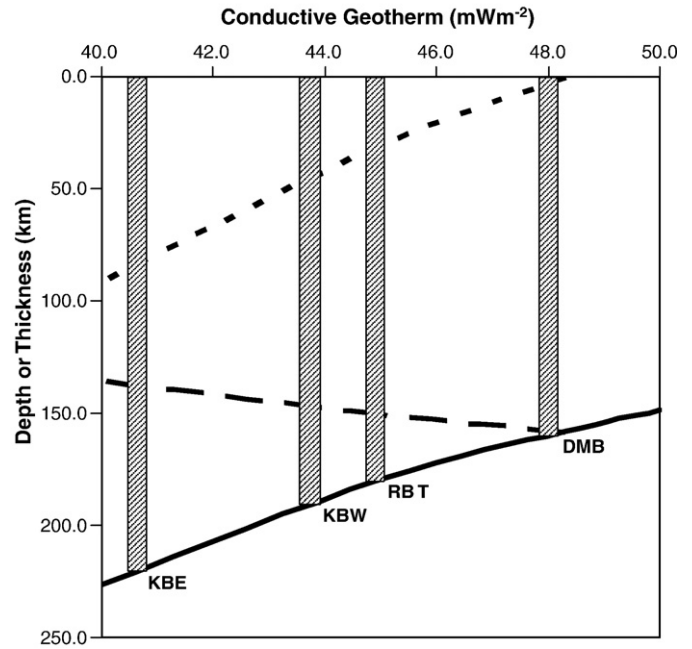


**Fig. 6.** Schematic illustration showing the depth to base of the lithosphere and top of the diamond stability field as a function of lithospheric mantle geotherm. The depth to the base of the lithosphere (solid line) is defined by the intersection of Pollack and Chapman (1977) geotherms with a mantle adiabat of potential temperature $T_P$ = 1300 °C, while the depth to the top of the diamond stability field (long dashed line) is defined by the intersection of the same geotherms with the graphite/diamond equilibrium of Kennedy and Kennedy (1976) (both as illustrated in Fig. 5). Thickness of the "diamond window" (short dashed line) is the difference between the previous two curves. A pressure-depth conversion factor equal to 3 km/kbar is assumed. Overlaid are present-day lithospheric thickness results (shaded vertical bars) for each terrane, derived from the MT electrical resistivity models. Terrane code names as for Fig. 3c.

Seismic body-wave tomography models (James et al., 2001; Fouch et al., 2004) agree with the MT observation that the lithosphere of the Western Kimberley Block is significantly different (warmer and thinner) when compared to the Eastern Kimberly Block. In the seismic models at 150 km and 300 km depths, there is a sharp transition to lower P- and S-wave velocities in the area of the Kaapvaal Craton below the Kheis Fold Belt, accounted for by either higher temperatures or less depleted compositions, or a combination of both. Similarly, although with lower lateral resolution, dispersion curves and maps of Rayleigh wave phase velocity, and modelled cross-sections of shear-wave velocity indicate lower lithospheric mantle velocities beneath the Kheis Belt when compared with the adjacent Kaapvaal Craton (Li and Burke, 2006). In the absence of lithospheric imaging below Kimberley, the MT model provides no insight into the possible tectonic relationship between the Western and Eastern Kimberley Blocks. As remarked in Section 2, it is unknown whether the two blocks were originally separate entities, but they were a coherent tectonic unit by 2.7 Ga at the latest. Whether the Western Kimberley Block consisted of thinner lithosphere at, or before, 2.7 Ga, or whether the lithosphere was thinned at a later stage, remains unconstrained.

The non-diamondiferous Gibeon and Gordonia kimberlite fields are located within the Rehoboth Terrane that is today characterised by lithosphere significantly thinner than that of the richly diamondiferous Eastern Kimberley Block. The ~80 km thickness of the "diamond window" below the Eastern Kimberley Block is reduced to ~30 km (65% reduction) below the Rehoboth Terrane (Fig. 6). Assuming that lithospheric thickness has not changed significantly since Mesozoic kimberlite eruption, the present-day thickness, and reduced depth extent into the diamond stability field, is able to account for the distribution of diamondiferous and non-diamondiferous kimberlite occurrences observed along and in the vicinity of profile KIM-NAM. In the light of the similarity in the width of the diamond widows of the Western

Kimberley Block and the Rehoboth Terrane, it will be worth noting in the future whether current exploration in the Tsabong area finds diamond grades adequate for mining.

In closure, we examine the notion that the Rehoboth Terrane might have, at some time in its past, been characterised by a "Kaapvaal-like" palaeo-geotherm (40–42 mW m$^{-2}$) and a thicker lithosphere structure required to support the geotherm (~210–220 km). The examination is made in the light of the Rehoboth's present-day thermal structure consisting of a ~45 mW m$^{-2}$ geotherm, a ~180 km lithospheric thickness, a relatively fertile chemical signature and the absence of diamondiferous kimberlites. When the Rehoboth Terrane might have acquired its cooler palaeo-geotherm is not well constrained. Bell et al. (2003) suggest that thermal "equilibration" of the subcontinent's geotherms occurred after the termination of the Namaqua orogenesis at ~1 Ga, when the entire subcontinent that had accreted around the core of the Kaapvaal Craton, including the Rehoboth Terrane, cooled to a "craton-like" thermal gradient of ~40 mW m$^{-2}$.

The lithospheric architecture of the Rehoboth Terrane in the depth range 180–210 km, required to support a cooler palaeo-geotherm, is unknown as no xenolith samples from deeper than 160 km are preserved in any of the Rehoboth kimberlites. (The absence of xenoliths from below 160 km depth is, in itself, suggestive of a lithosphere thickness not much greater than that at time of kimberlite eruption). It is possible that the Rehoboth Terrane acquired, during the "normal" course of its Proterozoic stabilisation and subsequent evolution, a ~210 km thick, depleted lithospheric section (perhaps more depleted than the present-day), commensurate with a "stable" ~41 mW m$^{-2}$ geotherm. Alternatively, in a more speculative model, a "transient" equilibration to a cooler conductive geotherm could possibly have been accommodated by a growth in lithospheric thickness through the accretion of a stagnant (i.e., non-convecting), cooled, little-depleted, asthenospheric-mantle layer at the base of the lithosphere. Initially, cooling of the stagnant layer would perturb the geotherm upwards in the overlying mantle, before equilibrating to a cooler one. Depleted lithospheric mantle in the first model would be stable and more difficult to displace at a later time by thermal and tectonic processes, being too buoyant for removal by gravitational forces and too refractory for assimilation and dispersal by melting (O'Reilly et al., 2001). Fertile mantle at the base of the lithosphere in the second model would be gravitationally unstable due to its very low buoyancy, and easier to remove by either melting or some mode of delamination.

In order to account for both the absence of diamonds and a hotter present-day thermal structure, any putative thicker, cooler lithospheric structure for the Rehoboth Terrane must have been thermally modified *at some time prior* to kimberlite eruption (75–65 Ma). How long before kimberlite eruption such a modification might have occurred is not constrained by this work. However, it should not have occurred too early, so as to disrupt the cool conductive geotherm in evidence in the upper lithospheric mantle. Bell et al. (2003) have inferred, from the disruption of the Gibeon xenolith *P–T* array at high temperatures, that the Rehoboth lithosphere experienced significant thermal perturbation either at, or shortly before, the time of kimberlite eruption. They propose a model in which the geotherm of the Rehoboth Terrane was elevated by the penetration of heat transporting magmas into shallow levels of the lithosphere during the widespread thermalism that affected the subcontinent during the Mesozoic. Furthermore, Bell et al. (2003) argue that Proterozoic lithosphere was more susceptible to melt penetration than its Archaean counterparts through being not thinner, but more fertile and structurally weakened by old tectonism. Their model, essentially one of *thermal advection* of heat into the lithosphere, is attractive in that if the magmatism was also associated with extensive lithospheric refertilisation, of which there is evidence in the Rehoboth lithosphere, it would help counter any isostatic (uplift) response to the decreasing thermal density of the lithosphere (by an increase in chemical density). Rather than significant uplift, the Rehoboth Terrane's recent

history appears to be characterised by the accumulation of sediments in the form of Carboniferous to Cretaceous Karoo sediments preserved in the Aranos basin (e.g., Tankard et al., 1982; Wanke, 2000) and Late Cretaceous to Recent Kalahari sediments preserved in the Kalahari Basin (Haddon, 2005). There is also no clear evidence of differential uplift of the Rehoboth Terrane with respect to the terranes on its margins. To account fully for the present-day lithospheric structure, however, some lithospheric thinning during the thermal/magmatic event is required. Such thinning though remains problematic as it would contribute significantly to the isostatic uplift. A model consisting only of *thermal conduction* of heat into the lithosphere above a mantle plume, without magmatic refertilisation, would appear to be a less viable model for raising the lithospheric geotherm in terms of the isostatic uplift that it would generate. However it does appear that thermal conduction alone would be able to deliver heat fast enough into the lithosphere: Sleep (2003) shows that thermal effect of a 40-km thick region of plume material ponded at the base of the lithosphere, with an excess temperature of 200 °C, would elevate lower mantle geotherms by 2 mW m$^{-2}$, and dissipate from the lower lithosphere in a period of about 60 million years (although it would take longer for the thermal anomaly to reach the surface). In a final alternative model that only applies to a gravitationally unstable lithospheric structure, such as the one described above, fertile lithospheric mantle might be *delaminated* to establish a thinner and hotter lithospheric structure. With the exception of the development of hotter geotherms, the other primary indicators of delamination — rapid regional uplift and the appearance of signature high-potassium magmas (Elkins-Tanton, 2005) — are not in clear evidence, and a delamination model does not appear to be reconcilable with the recent geological record for the Rehoboth Terrane.

## 6. Conclusion

Magnetotelluric profile KIM-NAM, in traversing the Eastern and Western Kimberley blocks, the Rehoboth Terrane and the Ghanzi-Chobe/Damara Belt, has revealed significant lateral variation in the electrical resistivity and thermal structure of the southern African subcontinent. There is a clear relationship between the bulk electrical resistivity of the lithosphere and the tectonic stabilisation-age of the terrane, as reflected in both crustal and lithospheric ages. The inferred present-day lithospheric geotherms are consistent with surface heat flow measurements and indicate that the latter are strongly controlled by variations in lithospheric thickness. The present-day geotherm of the Eastern Kimberley Block is very similar to that defined by xenoliths from Group 1 kimberlites (108–74 Ma), indicating that the thermal structure of the block has changed little since the time of kimberlite eruption. Chemical depletion in the lower lithospheric mantle of the Eastern Kimberley Block appears to be primarily defined by mantle refertilisation that occurred between the eruption of Group 2 and Group 1 kimberlites (Griffin et al., 2003; Kobussen et al., 2008). In contrast, the present-day geotherm of the Rehoboth Terrane is significantly hotter than that recorded in xenoliths from kimberlites erupted at ~70 Ma. The timing of the heating event that modified the earlier, cooler Rehoboth geotherm is not well constrained, but it must have pre-dated the eruption of the kimberlites to explain the absence of diamondiferous kimberlites in the terrane. A plausible model to account for the elevation of the Rehoboth palaeo-geotherm consists of the penetration of heat transporting magmas into the lithosphere at a very early stage of Mesozoic thermalism (Bell et al., 2003). Refertilisation of the lower lithospheric mantle during the thermalism would help to reduce the isostatic uplift of the resulting lithospheric structure. In such a model, the depth of the chemically depleted layer in the Rehoboth Terrane would, like the Eastern Kimberley Block, also be controlled by refertilisation. The advection of heat by magmas appears to have played an important part in the elevation of the lithospheric palaeo-geotherms in the region of kimberlite magmatism, in both the

Eastern Kimberley Block and the Rehoboth Terrane. Thermal modelling that accounts for the conduction and advection of heat into the lithosphere, and the isostatic response of potential lithospheric thickness changes and thermal and/or chemical density changes, is required to further constrain the temporal, thermal and chemical evolution of the Rehoboth Terrane.

## Appendix A References for geochemistry of xenolith samples used in Fig. 5

*Gibeon*

Boyd, F.R., Pearson, D.G., Hoal, K.O., Hoal, B.G., Nixon, P.H., Kingston, M.J., Mertzman, S.A., 2004. Garnet lherzolites from Louwrensia, Namibia: Bulk compositions and P/T relations. Lithos 77, 573–592.

Franz, L., Brey, G.P., Okrusch M., 1996. Steady state geotherm, thermal disturbances and tectonic development of the lower lithosphere underneath the Gibeon kimberlite province, Namibia. Contributions to Mineralogy and Petrology 126, 181–198.

Franz, L., Brey, G.P., Okrusch M., 1997. Metasomatic reequilibration of mantle xenoliths from the Gibeon kimberlite province (Namibia). Russian Geology and Geophysics 38, 261–276.

Mitchell, R.H., 1984. Garnet lherzolites from the Hanaus-I and Louwrensia kimberlites of Namibia. Contributions to Mineralogy and Petrology 86, 178–188.

*Kimberley*

Boyd, F.R., Nixon, P.H., 1978. Ultramafic nodules from the Kimberley pipes, South Africa. Geochimica et Cosmochimica Acta 42, 1367–1382 (Data Appendix).

Griffin, W.L., Shee, S.R., Ryan, C.G., Win, T.T., Wyatt, B.A., 1999. Harzburgite to lherzolite and back again: metasomatic processes in ultramafic xenoliths from the Wesselton kimberlite, Kimberley, South Africa. Contributions to Mineralogy and Petrology, 134, 232–250 (Data Appendix).

*Northern Lesotho*

Bloomer, A.G., Nixon, P.H., 1973. The geology of Letseng-la-terae kimberlite pipes. In: Nixon, P.H. (Ed.) Lesotho Kimberlites. Lesotho National Development Corporation, Maseru, pp. 20–36.

Carswell, D.A., Clarke, D.B., Mitchell, R.H., 1979. The petrology and geochemistry of ultramafic nodules from Pipe 200, Northern Lesotho. In: Boyd, F.R., Meyer, H.O.A. (Eds.), The Mantle Sample: Inclusions in Kimberlites and Other Volcanics. Proceedings Second International Kimberlite Conference, Volume 2, American Geophysical Union, Washington, D.C., pp. 127–144.

Cox, K.G., Gurney, J.J., Harte, B., 1973. Xenoliths from the Matsuko pipe. In: Nixon, P.H. (Ed.), Lesotho Kimberlites. Lesotho National Development Corporation, Maseru, pp. 76–100.

MacGregor, I.D., 1979. Mafic and ultramafic xenoliths from the Kao kimberlite pipe. In: Boyd, F.R., Meyer, H.O.A. (Eds.), The Mantle Sample: Inclusions in Kimberlites and Other Volcanics. Proceedings Second International Kimberlite Conference, Volume 2, American Geophysical Union, Washington, D.C., pp. 156–172.

Mofokeng, S.W., 1998. A comparison of the nickel and the conventional geothermometers with respect to the Jagersfontein and the Matsoku kimberlite peridotite xenoliths. Unpublished M.Sc. Thesis, University of Cape Town, 124 pp.

Nixon, P.H., 1987. Kimberlitic xenoliths and their cratonic setting. In: Nixon, P.H. (Ed.), Mantle Xenoliths. John Wiley & Sons, pp. 215–239.

Nixon, P.H., Boyd, F.R., 1973. Petrogenesis of the granular and sheared ultrabasic nodules suite in kimberlites. In: Nixon, P.H. (Ed.), Lesotho Kimberlites. Lesotho National Development Corporation, Maseru, pp. 48–56.

Simon, N.S.C., Irvine, G.J., Davies, G.R., Pearson, D.G., Carlson, R.W., 2003. The origin of garnet and clinopyroxene in "depleted" Kaapvaal peridotites. Lithos 71, 289–322.

*Kimberley and Northern Lesotho*

Delaney, J.S., Smith, J.V., Carswell, D.A., Dawson, J.B., 1980. Chemistry of micas from kimberlites and xenoliths — II. Primary- and secondary-textured micas from peridotite xenoliths. Geochimica et Cosmochimica Acta 44, 857–872. (Data Appendix).

Delaney, J.S., Smith, J.V., Dawson, J.B., Nixon, P.H., 1979. Manganese thermometer for mantle peridotites. Contributions to Mineralogy and Petrology 71, 157–169.

Griffin, W.L., Cousens, D.R., Ryan, C.G., Sie, S.H., Suter, G.F., 1989. Ni in chrome pyrope garnets: a new geothermometer. Contributions to Mineralogy and Petrology 103, 199–202.

Hervig, R.L., Smith, J.V., Dawson, J.B., 1986. Lherzolite xenoliths in kimberlites and basalts: petrogenetic and crystallographic significance of some minor and trace elements in olivine, pyroxenes, garnet and spinel. Transactions Royal Society of Edinburgh (Earth Sciences) 77, 181–201.

Luth, R.W., Virgo, D., Boyd, F.R., Wood, B.J., 1990. Ferric iron in mantle-derived garnets: Implications for thermobarometry and for the oxidation state of the mantle. Contributions to Mineralogy and Petrology 104, 56–72.

Pearson, D.G., Boyd, F.R., Haggerty, S.E., Pasteris, J.D., Field, S.W., Nixon, P.H., Pokhilenko, N,P., 1994. The characterization and origin of graphite in cratonic lithospheric mantle: a petrological carbon isotope and Raman spectroscopic study. Contributions to Mineralogy and Petrology 115, 449–466.

Pearson, D.G., Boyd, F.R., Nixon, P.H., 1990. Graphite-bearing mantle xenoliths from the Kaapvaal craton: implications for graphite and diamond genesis. Annual Report, Director of Geophysical Laboratory, Carnegie Institute Washington, pp. 11–19.

Smith, D., Boyd, F.R., 1992. Compositional zonation in garnets in peridotite xenoliths. Contributions to Mineralogy and Petrology 112, 134–147.

## References

Allsopp, H.L., Barrett, D.R., 1975. Rb–Sr age determinations on South African kimberlite pipes. Physics and Chemistry of the Earth 9, 605–617.

Allsopp, H.L., Bristow, J.W., Smith, C.B., Brown, R., Gleadow, A.J.W., Kramers, J.D., Garvie, O.G., 1989. A summary of radiometric dating methods applicable to kimberlites and related rocks. In: Ross, J. (Ed.), Kimberlites and Related Rocks, Vol. 1: Geological Society of Australia Special Publication, vol. 14, pp. 343–357.

Appleyard, C.M., Bell, D.R., le Roux, A.P., 2007. Petrology and geochemistry of eclogite xenoliths from the Rietfontein kimberlite, Northern Cape, South Africa. Contributions to Mineralogy and Petrology 154, 309–333.

Baumgartner, M.C., le Roex, A.P., Gurney, J.J., 2000. Mantle and crustal xenoliths from the Okenyenya lamprophyre diatreme: constraints on the upper mantle and lower crust beneath the Damara Belt, northwestern Namibia. Henno Martin Special, vol. 12. Communications, Geological Survey of Namibia, pp. 279–290.

Becker, T., Hansen, B.T., Weber, K., Wiegand, B., 2004. Isotope systematics (Sm/Nd, Rb/Sr, U/Pb) of the Elim Fm, the Alberta Complex, and the Weener Igneous Complex — probable genetic links between magmatic rocks of the Paleoproterozoic Rehoboth Basement Inlier/Namibia. Communications Geological Survey of Namibia 13, 75–84.

Bell, D.R., Schmitz, M.D., Janney, P.E., 2003. Mesozoic thermal evolution of the southern African mantle lithosphere. Lithos 71, 273–287.

Boyd, F.R., Pearson, D.G., Hoal, K.O., Hoal, B.G., Nixon, P.H., Kingston, M.J., Mertzman, S.F., 2004. Garnet lherzolites from Louwrensia, Namibia: bulk composition and P/T relations. Lithos 77, 573–592.

Brey, G.P., Köhler, T., Nickel, K.G., 1990. Geothermobarometry in Four-phase Lherzolites I. Experimental results from 10 to 60 kb. Journal of Petrology 31, 1313–1352.

Constable, S.C., 2006. SEO3: a new model of olivine electrical conductivity. Geophysical Journal International 166, 435–437.

Constable, S.C., Shankland, T.J., Duba, A., 1992. The electrical conductivity of an isotropic olivine mantle. Journal of Geophysical Research 97, 3397–3404.

Davies, G.R., Spriggs, A.J., Nixon, P.H., 2001. A non-cognate origin for the Gibeon kimberlite megacryst suite, Namibia: implications for the origin of Namibian kimberlites. Journal of Petrology 42, 159–173.

Davis, G.L., 1977. The ages and uranium content of zircons from kimberlites and associated rocks. Carnegie Institute Washington Yearbook 76, 631–635.

Davis, G.L., Krogh, T.E., Erlank, A.J., 1976. The ages of zircons from kimberlites from South Africa. Carnegie Institute Washington Yearbook 75, 821–824.

Dawson, J.B., 1989. Geographic and time distribution of kimberlites and lamproites: relationships to tectonic processes. In: Ross, J., Jaques, A.L., Ferguson, J., Green, D.H., O'Reilly, S.Y., Danchin, R.V., Janse, A.J.A. (Eds.), Kimberlites and related rocks: their composition, occurrence and emplacement. Geological Society of Australia Special Publication, vol. 14. Blackwell, Carlton, pp. 323–342.

de Wit, M.J., Tinker, J.H., 2004. Crustal structure across the central Kaapvaal Craton from deep-seismic reflection data. South African Journal of Geology 107, 185–206.

de Wit, M.J., Roering, C., Hart, R.J., Armstrong, R.A., de Ronde, C.E.J., Green, R.W.E., Tredoux, M., Peberdy, E., Hart, R.A., 1992. Formation of Archaean continent. Nature 357, 553–562.

de Wit, M.J., Richardson, S.H., Ashwal, L.D., 2004. Kaapvaal Craton special volume — an introduction. South African Journal of Geology 107, 1–6.

Elkins-Tanton, L.T., 2005. Continental magmatism caused by lithospheric delamination. In: Foulger, G.R., Natland, J.H., Presnall, D.C., Anderson, D.L. (Eds.), Plates, Plumes and Paradigms. Special Paper, vol. 338. Geological Society of America, pp. 449–461.

Faure, S., 2006. World Kimberlites and Lamproites CONSOREM Database (Version 2006-1). Consortium de Recherche en Exploration Minérale. Université du Québec à Montréal. www.consorem.ca.

Finnerty, A.A., 1989. Xenolith-derived mantle geotherms: whither the inflection? Contributions to Mineralogy and Petrology 102, 367–375.

Fouch, M.J., James, D.E., VanDecar, J.C., van der Lee, S., Kaapvaal Seismic Group, 2004. Mantle seismic structure beneath the Kaapvaal and Zimbabwe Cratons. South African Journal of Geology 107, 33–44.

Griffin, W.L., O'Reilly, S.Y., Natapov, L.M., Ryan, C.G., 2003. The evolution of lithospheric mantle beneath the Kalahari Craton and its margins. Lithos 71, 215–241.

Groom, R.W., Bailey, R.C., 1989. Decomposition of magnetotelluric impedance tensors in the presence of local three-dimensional galvanic distortion. Journal of Geophysical Research 94, 1913–1925.

Grütter, H., Moore, R., 2003. Pyroxene geotherms revisited — an empirical approach based on Canadian xenoliths. Extended Abstract, 8th International Kimberlite Conference, Canada.

Grütter, H.S., Apter, D.B., Kong, J., 1999. Crust–Mantle coupling: Evidence from mantle-derived xenocrystic garnets: Proceedings 7th International Kimberlite Conference, vol. 1, pp. 307–313.

Grütter, H., Latti, D., Menzies, A., 2006. Cr-saturation arrays in concentrate garnet compositions from kimberlite and their use in mantle barometry. Journal of Petrology 47, 801–820.

Gurney, J.J., 1984. A correlation between garnets and diamonds. In: Glover, J.E., Harris, P.G. (Eds.), Kimberlite occurrence and origin: a basis for conceptual models in exploration. University of Western Australia Publication, vol. 8. Geology Department and University Extension, pp. 143–166.

Gurney, J.J., Mathias, M., Siebert, C., Mosely, G., 1971. Kyanitic eclogites from the Rietfontein Kimberlite Pipe, Mier Coloured Reserve, Gordonia, Cape Province, South Africa. Contributions to Mineralogy and Petrology 30, 46–52.

Gutzmer, J., Beukes, N.J., Pickard, A., Barley, M.E., 2000. 1170 Ma SHRIMP age for the Koras Group bimodal volcanism, Northern Cape province. South African Journal of Geology 103, 32–37.

Haddon, G.I., 2005. The Sub-Kalahari Geology and Tectonic Evolution of the Kalahari Basin, Southern Africa. Unpublished Ph.D. thesis, University of the Witwatersrand, Johannesburg.

Hartnady, C.H., Joubert, P., Stowe, C., 1985. Proterozoic crustal evolution in southwestern Africa. Episodes 8, 236–243.

Heinson, G., White, A., 2005. Electrical resistivity of the Northern Australian lithosphere: crustal anisotropy or mantle heterogeneity? Earth and Planetary Science Letters 232, 157–170.

Hoal, B.G., Hoal, K.E.O., Boyd, F.R., Pearson, D.G., 1995. Age constraints on crustal and mantle lithosphere beneath the Gibeon kimberlite field, Namibia. South African Journal of Geology 98, 112–118.

Jacobs, J., Pisarevsky, S., Thomas, R.J., Becker, T., 2008. The Kalahari Craton during the assembly and dispersal of Rodinia. Precambrian Research 160, 142–158.

James, D.E., Fouch, M.J., VanDecar, J.C., van der Lee, S., Kaapvaal Seismic Group, 2001. Tectospheric structure beneath southern Africa. Geophysical Research Letters 28, 2485–2488.

Jelsma, H.A., de Wit, M., Thiart, C., Dirks, P.H.G.M., Viola, G., Basson, I.J., Anckar, E., 2004. Preferential distribution along transcontinental corridors of kimberlites and related rocks of Southern Africa. South African Journal of Geology 107, 301–324.

Jones, A.G., 1983. On the equivalence of the "Niblett" and "Bostick" transformations in the magnetotelluric method. Journal of Geophysics 53, 72–73.

Jones, A.G., 1999. Imaging the continental upper mantle using electromagnetic methods. Lithos 48, 57–80.

Jones, A.G., Chave, A.D., Egbert, G., Auld, D., Bahr, K., 1989. A comparison of techniques for magnetotelluric response function estimation. Journal of Geophysical Research 94, 14201–14213.

Jones, A.G., Lezaeta, P., Ferguson, I.J., Chave, A.D., Evans, R.L., Garcia, X., Spratt, J., 2003. The electrical structure of the Slave craton. Lithos 71, 505–527.

Jones, A.G., Evans, R.L., Eaton, D.W., 2009. Velocity–conductivity relationships for mantle mineral assemblages in Archean cratonic lithosphere based on a review of laboratory data and Hashin–Shtrikman extremal bounds. Lithos 109, 131–143.

Jones, A.G., et al., 2009, this issue. Area selection for diamonds using magnetotellurics: Examples from southern Africa. Proceedings of the 9th International Kimberlite Conference. Lithos 112S, 083–092.

Jones, M.Q.W., 1998. A Review of Heat Flow in Southern Africa and the Thermal Structure of the Lithosphere. In: South African Geophysical Review, vol. 2. South African Geophysical Association, pp. 115–122.

Karato, S., 1990. The role of hydrogen in the electrical conductivity of the upper mantle. Nature 347, 272–273.

Karato, S., 2006. Remote sensing of hydrogen in Earth's mantle, Water in Nominally Anhydrous Minerals. Reviews in Mineralogy & Geochemistry 62, 343–375.

Kennedy, C.S., Kennedy, G.C., 1976. The equilibrium boundary between graphite and diamond. Journal of Geophysical Research 81, 2467–2470.

Kobussen, A.F., Griffin, W.L., O'Reilly, S.Y., Shee, S.R., 2008. Ghosts of lithospheres past: imaging an evolving lithospheric mantle in Southern Africa. Geology 36, 515–518.

Korja, T., 2007. How is the European lithosphere imaged by magnetotellurics? Surveys in Geophysics 28, 239–272.

Li, A., Burke, K., 2006. Upper mantle structure of southern Africa from Rayleigh wave tomography. Journal of Geophysical Research 111, B10303. doi:10.1029/2006JB004321.

MacGregor, I.D., 1974. The system MgO–Al$_2$O$_3$–SiO$_2$: solubility of Al$_2$O$_3$ in enstatite for spinel and garnet peridotite compositions. American Mineralogist 59, 110–119.

Maumus, J., Bagdassarov, N., Schmeling, H., 2005. Electrical conductivity and partial melting of mafic rocks under pressure. Geochimica et Cosmochimica Acta 69, 4703–4718.

McNeice, G.W., Jones, A.G., 2001. Multisite, multi-frequency tensor decomposition of magnetotelluric data. Geophysics 66, 158–173.

Modie, B.N., 2000. Geology and mineralisation in the Meso- to Neoproterozoic Ghanzi-Chobe Belt of northwest Botswana. Journal of African Earth Sciences 30, 467–474.

Nagel, R., Warkus, F., Becker, T., Hansen, B.T., 1996. U–Pb-Zirkondatierungen der Gaub Valley Formation am Südrand des Damara Orogens-Namibia und ihre Bedeutung für die Entwicklung des Rehoboth Basement Inlier. Zeitschrift für Geologische Wissenschaft 24, 611–618.

Nickel, K.G., Green, D.H., 1985. Empirical geothermobarometry for garnet peridotites and implications for the nature of the lithosphere, kimberlites and diamonds. Earth and Planetary Science Letters 73, 158–170.

Nimis, P., Taylor, W.R., 2000. Single clinopyroxene thermobarometry for garnet peridotites. Part 1. Calibration and testing of a Cr-in-Cpx barometer and an enstatite-in-Cpx thermometer. Contributions to Mineralogy and Petrology 139, 541–554.

O'Reilly, S.Y., Griffin, W.L., Poudjom Djomani, Y.H., Morgan, P., 2001. Are lithospheres forever? Tracking changes in subcontinental lithospheric mantle through time. GSA Today April 2001, 4–10.

Pollack, H.N., Chapman, D.S., 1977. On the regional variation of heat flow, geotherms, and lithospheric thickness. Tectonophysics 38, 279–296.

Prave, A.R., 1996. Tale of three cratons: tectonostratigraphic anatomy of the Damara orogen in northwestern Namibia and the assembly of Gondwana. Geology 24, 1115–1118.

Rodi, W., Mackie, R.L., 2001. Nonlinear conjugate gradients algorithm for 2-D magnetotelluric inversion. Geophysics 66, 174–187.

Rudnick, R., Nyblade, A.A., 1999. The thickness and heat production of Archean lithosphere: Constraints from xenolith thermobarometry and surface heat flow. In: Fei, Y., Bertka, C., Mysen, B.O. (Eds.), Mantle Petrology: Field Observations and High Pressure Experimentation: A Tribute to Francis R. (Joe) Boyd. The Geochemical Society Special Publication, vol. 6. University of Pennsylvania, pp. 3–12.

Schmitz, M.D., Bowring, S.A., de Wit, M.J., Gartz, V., 2004. Subduction and terrane collision stabilise the western Kaapvaal craton tectosphere 2.1 billion years ago. Earth and Planetary Science Letters 222, 363–376.

Simpson, F., Bahr, K., 2005. Practical Magnetotellurics. Cambridge University Press, p. 270.

Sleep, N.H., 2003. Geodynamic implications of xenolith geotherms. Geochemistry Geophysics Geosystems 4, 1079. doi:10.1029/2003GC000511.

Spriggs, A.J., 1988. An isotopic and geochemical study of kimberlites and associated alkaline rocks from Namibia. Unpublished PhD Thesis, University of Leeds, UK.

Tankard, A.J., Jackson, M.P., Eriksson, E.K.A., Hobday, D.K., Hunter, D.R., Minter, W.E.L., 1982. Crustal Evolution of Southern Africa. InSpringer, Berlin, p. 523.

Tinker, J.H., de Wit, M.J., Royden, L.H., 2004. Old, strong continental lithosphere with weak Archaean margin at ~1.8 Ga, Kaapvaal Craton, South Africa. South African Journal of Geology 107, 255–260.

Wanke, A., 2000. Karoo-Etendeka Unconformities in NW Namibia and their Tectonic Implications. Unpublished Ph.D. thesis, Julius-Maximilians University, Würzburg.

Wessel, P., Smith, W.H.F., 1991. Free software help map and display data. EOS Transactions American Geophysical Union 72, 441.

Wessel, P., Smith, W.H.F., 1998. New, improved version of the Generic Mapping Tools released. EOS Transactions American Geophysical Union 79, 579.

Whitehead, K., le Roex, A., Class, C., Bell, D., 2002. Composition and Cretaceous thermal structure of the upper mantle beneath the Damara Mobile Belt: evidence from nephelinite-hosted peridotite xenoliths, Swakopmund, Namibia. Journal of the Geological Society London 159, 307–321.

Xu, Y.S., Shankland, T.J., 1999. Electrical conductivity of orthopyroxene and its high pressure phases. Geophysical Research Letters 26, 2645–2648.

Xu, Y.S., Shankland, T.J., Duba, A.G., 2000. Pressure effect on electrical conductivity of mantle olivine. Physics of the Earth and Planetary Interiors 118, 149–161.

Ziegler, U.R.F., Stoessel, G.F.U., 1991. Note: New constraints on the age of the Weener Intrusive Suite, the Gamsberg Granite and the crustal evolution of the Rehoboth Basement Inlier, Namibia. Communications Geological Survey of Namibia 7, 75–78.